Analyst

Accepted Manuscript

This is an *Accepted Manuscript*, which has been through the Royal Society of Chemistry peer review process and has been accepted for publication.

Accepted Manuscripts are published online shortly after acceptance, before technical editing, formatting and proof reading. Using this free service, authors can make their results available to the community, in citable form, before we publish the edited article. We will replace this *Accepted Manuscript* with the edited and formatted *Advance Article* as soon as it is available.

You can find more information about *Accepted Manuscripts* in the Information for Authors.

Please note that technical editing may introduce minor changes to the text and/or graphics, which may alter content. The journal's standard Terms & Conditions and the Ethical guidelines still apply. In no event shall the Royal Society of Chemistry be held responsible for any errors or omissions in this *Accepted Manuscript* or any consequences arising from the use of any information it contains.

1
2
3
4
5
6
7
8
9
10
11
12
13
14
15
16
17
18
19
20
21
22
23
24
25
26
27
28
29
30
31
32
33
34
35
36
37
38
39
40
41
42
43
44
45
46
47
48
49
50
51
52
53
54
55
56
57
58
59
60

Single Molecule Analysis by Biological Nanopore Sensors

Yi-Lun Ying, Chan Cao and Yi-Tao Long*

This mini review will discusses current strategies for the analysis of an individual analyte in the field of nanopore biosensors.

Journal Name
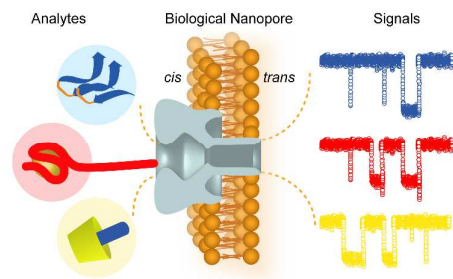
ARTICLE

Single Molecule Analysis by Biological Nanopore Sensors

Yi-Lun Ying, Chan Cao and Yi-Tao Long*

Nanopore sensors provide a highly innovative technique for the rapid and label-free single molecule analysis, which hold the great potential in routing applications. Biological nanopores have been used as ultra-sensitive sensors over wide ranges of single molecule analysis including DNA sequencing, disease diagnosis, drug screening, environment monitoring and the construction of molecule machine. This mini review will focus on the current strategies for the identification and characterization of an individual analyte, especially based on our recent achievements in biological nanopore biosensors.

1. Introduction

In the past two decades, biological nanopore sensors have emerged as a new powerful tool to sense single molecules. The concept of biological nanopore sensors was first proposed in 1996 by using an α-hemolysin (α-HL) which consists of a narrowest constriction of 1.4 nm. [1,2] If a charged biopolymer is electrophoretically driven through a biological nanopore by an applied electric potential across the membrane, it produces measurable transient modulation in the ionic current passing through the pore. By monitoring the blockage currents, the properties of an individual biopolymer can be read off in an ultrafast way.[3,4] Herein, biological nanopores display as unique single molecule sensors with the advantages of detection in high-throughput and no requirements for labeling/immobilization in most cases.[5]

Since biological nanopores exhibit the well-controlled geometry and reproducible chemical structure, they provide the excellent reproducibility and high sensitivity for single molecule analysis. The structure of a biological nanopore can be precisely manipulated by site-directed mutagenesis and the targeted chemical modification.[6-11] Among all the selected biological nanopores, α-HL nanopore becomes the preferred choice in the field of biological nanopores because of its appropriate inner diameter and repeatable self-assembly ability. As shown in Fig. 1, the typical experimental set-up for a α-HL nanopore is that a small orifice (usually varied from 25 μm to 250 μm) located in a thin barrier that separated two compartments (henceforth called *cis* and *trans*). Electrolyte buffer is added into each compartment and the lipid bilayer is formed across the orifice. The constant potential is applied by two integrate Ag/AgCl electrodes, which are the most frequently used for driving the molecules to thread through the pore. In general, a single α-HL pore in a buffer containing 1 M KCl at an applied potential of +100 mV across the membrane produces a current of +100 pA which is conveniently measured by a current amplifier. Under open pore conditions, the ionic

current is due to the enhanced transport of K^+ ions compared to the much larger Cl^- ions. Generally, blockages for the given analyte can be characterized by three parameters: blockage current, blockage duration and the time interval between two blockages. Since each type of analytes gives rise to specific modulations, these three parameters can be used in the analysis of biological nanopores in most of cases.
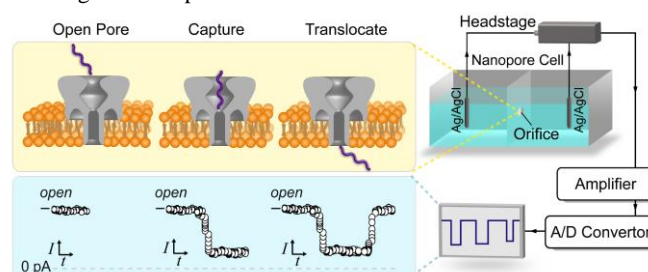

Fig. 1 Model illustrating the principle and experimental configuration of the α-HL nanopore sensors by taking an example of single-stranded DNA (ssDNA) analysis. The open-state of an α-HL pore exhibits stable open pore current. When an individual ssDNA enters into an α-HL pore, it causes the decrease of the ionic current from its initial open pore current. Then, ssDNA transverses through the α-HL pore resulting in a measurable blockage current and duration. Eventually, ssDNA translocates through the pore and the ionic current returns to the open pore state. In the experimental configuration of biological nanopore, an orifice in the nanopore chamber is used to support the bilayer which is inserted by a biological nanopore. The ionic current is measured by an ultra-sensitive current amplifier and then converted into digital signals by an analogy-to-digital convertor. The current traces are displayed by a monitor.

The biological nanopores have been used over wide ranges of single molecule analysis such as DNA sequencing[12], DNA damages analysis[13-16], disease-associate targets identifications[17,

[18], metal ions discriminations[7, 19, 20] and probing the structures of proteins[21-25]. Several reviews have been published for the biological nanopore sensors in the view of the applications where the readers will have a tutorial and elaborate overview.[12, 26-30] Herein, this mini review will focus on discussing the analysis strategies for the identification and characterization of an individual analyte, especially based on our recent achievements in biological nanopore biosensors.

2. Nucleic acid aptamers incorporated nanopore detections

Since the crystal structure of α-HL was solved in 1996, it has been widely used in the nanopore detection of nucleic acids. The mushroom-shaped channel consists of a cap domain outside the membrane and a 14-stranded β-barrel entry as the lumen. After assembly from the seven monomers in the membrane, the cap domain with a large vestibule faces the *cis* side of the membrane and the β-barrel faces the *trans* side. In most of the nanopore experiments, the nucleic acids are driven into the α-HL nanopore from the *cis* side under the applied potential. A vestibule of α-HL connects to a constriction with an internal diameter of about 1.4 nm, allowing the translocation of single-strand DNA (ssDNA) or RNA in its linear form. It should be noted that α-HL has a wide *cis* side opening of 2.6 nm diameter and a 4.6 nm maximum diameter vestibule. Therefore, α-HL could capture the nucleic acids in their varied conformations such as hairpin and G-quadruplex under the applied potential, more than the linear form. After entering into the vestibule of α-HL, a nucleic acid strand would adjust itself for the successive translocation. For example, poly(dT) induced a distinct double-step blockage current due to its poor stacking of thymine residues (Fig. 2a-b).[31-33] At first, the free jointed chain of poly(dT)$_{45}$ enters the vestibule under an applied potential resulting in a partial blockage current (level I). Then, poly(dT)$_{45}$ remains resident in the vestibule area to extend itself for exploring the narrow entrance of the stem, which contributes to the duration of level I. Once the leading part finds the access, poly(dT)$_{45}$ immediately threads through the stem of the pore resulting in a further increase in the blockage current labeled as level II. In order to decrease entropic barrier for the translocation of poly(dT)$_{45}$, the antigen binding fragment Fab HED10 was introduced to accelerate the translocation of poly(dT)$_{45}$.[34] Fab HED10 acts as a rudder forcing the poly(dT)$_{45}$ into an extended and linear conformation (Fig. 2a), which decreases the time required to find the entrance to the narrow constriction of the pore (Fig. 2c).[34]

A nucleic acid aptamer which spontaneously forms a secondary structure is capable of selectively binding an analyte. Since the entropic barrier required to linearize a nucleic acid aptamer is one of the dominant contributions to the entire energy barrier of the translocation, a nucleic acid aptamer undergoes the conformational changes inside the cavity of α-HL resulting in the characteristic and distinguishable signals. The conformational change process of the nucleic acid aptamer was first studied by encapsulating a single thrombin-binding aptamer (TBA) in the cavity of an α-HL nanopore. [35, 36] TBA G-quadruplex experiences a spontaneous unfolding process before traversing through the α-HL, which results in a distinguishable blockage current (Fig. 2d).

The conformation of an nucleic acid aptamer is the key to specific binding of its target molecule, even in the case of very closely related targets. If nucleic acid aptamers could be designed as a probe for improving the selectivity of biological

nanopore sensors, a biological nanopore should display its ability in the identification of the target-induced conformational changes of a nucleic acid aptamer. Recently, our group discriminated the conformational changes of the ATP-binding DNA aptamer (ABA) by an α-HL nanopore when the aptamer bound different targets (Fig. 2e).[37] At first, upon annealing, the
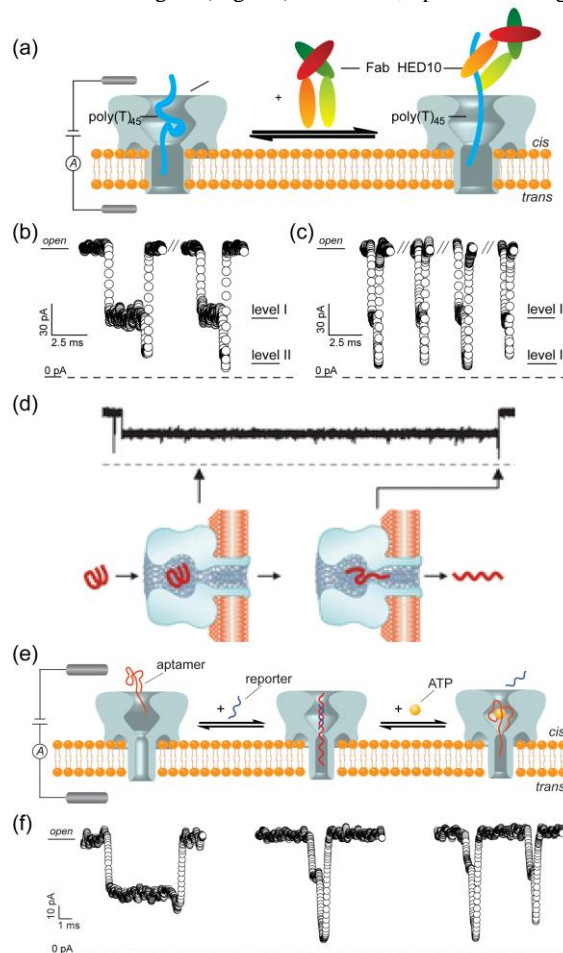

Fig. 2 (a) The mechanism for poly(dT)$_{45}$ specific binding with Fab HED10. The Fab HED10 acts as a rudder to steer the poly(dT)$_{45}$ into the pore. (b) The typical current traces of poly(dT)$_{45}$ translocation events. (c) The typical current traces of poly(dT)$_{45}$ translocation events in the presence of Fab HED10. Each event is divided into two blockage levels. The smaller blockade is labeled as level I and the deeper blockade is assigned to level II. (d) Current traces and model showing the encapsulation of a TBA G-quadruplex in an α-HL followed by the spontaneous unfolding process in 1M KCl. (e) The α-HL analysis of conformational changes of ABA induced by the targets. A folded ABA strand converts into a double strand by a reporter strand. In the presence of ATP, ABA changes into a new conformation with bound ATP and causes the reporter to be released. (f) The characteristic blockages for an ABA in its folded, double strand and ATP-bound form, respectively. Modified with the permission from Ref. 34, 35 and 37.

linear DNA strand folds into its secondary structure resulting in its ATP-recognition conformation. A folded aptamer enters the vestibule generating a characteristic signal which is described as a step followed by a spike (Fig. 2f). This current shape suggested that the captured aptamer remains resident in the vestibule area until the secondary structure is partially broken

and the threading strand is trying to transport through the pore resulting in a further increase in current blockage. The duration of the "step" represents the time needed for unfolding the aptamer. Then, the folded aptamer sequence was exposed to a complementary strand (14-mer DNA strand, reporter) and ATP, respectively. The typical current traces of both ABA:reporter and ABA:ATP in Fig. 2f show the partial current blockage followed by a terminal spike. Although folded ABA, ABA:reporter and ABA:ATP generate the similar shape of the events as "step-spike", there are clear differences: first, the blockage current of "spike" during the recording of ABA at 15 °C are about 60% (± 3%) to the open pore current while both ABA:reporter and ABA:ATP produces a deeper "spike". This difference indicates that the folded ABA would exit out of the pore from *cis* side in its partially unfolded state while both ABA:reporter and ABA:ATP translocate through the pore after completing their unzipping/unfolding processes in the vestibule, respectively. Second, the lifetime of the ABA:ATP complex (0.29 ms) and ABA:reporter complex (0.50 ms) are shorter than the partially unfolding time of ABA (4.17 ms). Therefore, the binding of a target weakens the interactions holding the secondary structure of ABA together and results in a faster unfolding/unzipping time. Third, the frequency of transit events is much higher for the ABA:ATP complex (13 s^{-1}) compared with ABA:reporter duplex (3 s^{-1}). Therefore, the nanopore allows for the detection of an ATP-binding aptamer in its folded, ATP-bound and linear conformations based on the unique combinations of duration times, blockage shapes and event frequencies. Competition assays, between the ABA:ATP and ABA:reporter complexes, were carried out and the results illustrated that the frequency of translocation events after competition occurring is about 3.5 times higher than the first minute after the competition began. Therefore, our contribution demonstrates that nanopore biosensors can be utilized for the real-time discrimination of the different forms of aptamer as well as detection of competing targets.

The incorporation of aptamer probe would greatly improve the selectivity of the biological nanopore sensors. Recently, a thrombin-binding aptamer was covalently attached to a cysteine residue near the *cis* entrance of α-HL through a disulfide bound.[38] The binding of thrombin to the aptamer alters the ionic current through the pore. This aptamer modified α-HL allowed the detection of nanomolar concentration of thrombin.

Furthermore, the α-HL nanopore was applied to study the photo-regulated interactions between RNA aptamer and photochromic spiropyran (Fig. 3a).[39] The characteristic blockage of RNA aptamer illustrates the typical three levels which are Level 1 (L1), Level 2 (L2) and Level 3 (L3), respectively (Fig. 3b). RNA aptamer could specifically bind with closed form of spiropyrans. Although the addition of spiropyran scarcely alters the conformation of RNA aptamer, the durations of the L1 and L2 show the significantly increase comparing to the value of RNA aptamer only. The interactions between RNA aptamer and spiropyran produce an intermediate logging in the cavity of α-HL. After irradiation of UV light (λ=365 nm), the ring-closed spiropyran photo-isomerized to merocyanine, which is unable to bind with RNA aptamer.[40] The duration time of RNA/merocyanine is consistent with that of RNA aptamer only, rather than the RNA: spiropyran complex (Fig. 3c). Consequently, the two photo-isomers spiropyran and merocyanine could be readily determined by α-HL nanopore at single-molecule level upon tuning the translocation process of RNA aptamer.
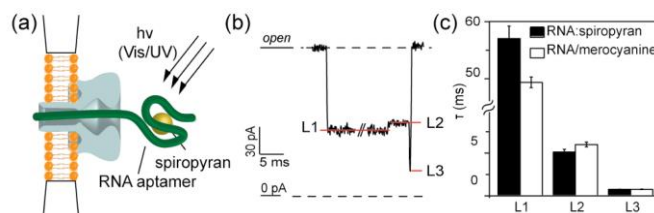

Fig. 3 (a) Translocation of an an RNA:spiropyran through the α-HL. (b) A typical three-level event for spiropyran RNA aptamer. (c) Durations of each level of the typical current traces after irradiation with visible light (λ>490 nm) and UV light (λ=365 nm). Reproduced with the permission from Ref. 39.

Besides the interactions between aptamer and target, the conformational changes of oligonucleotides induced by the ions could also be employed in the nanopore detections of heavy ions.[19, 20, 41] For example, a mercury (Hg^{2+}) sensing platform based on the T-Hg^{2+}-T paring was carried out by an α-HL nanopore.[20] Comparing to the ssDNA probe alone, a stable hairpin structure of ssDNA probe mediating by Hg^{2+} induced the longer translocation time. From the 2D-events contour plots, the presences of Hg^{2+} can be detected within 30 min at ~ 7 nm. The simultaneously identification of Pb^{2+} and Ba^{2+} was further achieved by incorporated G-quadruplex DNA-based probe.[19]

3. Host-guest interactions assisted nanopore detections

The host molecules including cyclodextrins, calixarenes, cucurbiturils etc. recognize guest molecules through noncovalent bonding. On the one hand, the host molecule existing within the pore alters the magnitude of ion conductance under an applied potential. On the other hand, the host molecule acts as a specific binding site for the guest analyte. Thus, the host-guest interactions not only improve the current resolution but also endow the nanopore with the selectivity in single molecule analysis. The pioneer works which integrated host-guest interactions with α-HL nanopore were carried out by Bayley's group.[42-44] They showed that β-cyclodextrins (βCD, cavity diameter ≈ 0.6 nm) and its derivatives could lodge in the lumen of a mutant α-HL. The βCD forms a "nanocavity" inside the α-HL, where the trapping, reaction and releasing of the guest molecules could induce the clear current differences.[44] In their later work, the positively charged βCD which was combined with a mutant α-HL partially obstructed the pore to distinguish four dNMPs.[45] The exonuclease cleaved the deoxynucleoside monophosphates (dNMPs) off the end of an ssDNA strand, and then the dNMPs were successively trapped inside the βCD resulting in the different levels of the current blockages. To improve the stability of the nanopore sensor, a βCD has been covalently attached within the lumen of the mutant α-HL.[46] Therefore, this stable nanopore biosensor has achieved to discriminate dNMPs cleaved from ssDNA by exonuclease. By virtue of the nanocavity provided by βCD, the average accuracy of this detection system could reach to 99.8% for identifying unlabeled nucleoside molecules.[47]

Two ring-expanded, disulfide-linked stereoisometic skeleton of CDs were further modified to finely modulate binding selectivity of sodium deoxycholate inside α-HL.[48] Besides, the γ-cyclodextrin (γCD) was lodged in the α-HL nanopore.[49] By monitoring the current traces through the γCD functionalized α-HL, the host-guest interactions of the γCD with adamatane carboxylate (AD) were resolved. The results demonstrated that this functionalized nanopore was sensitive to reveal the salts

effect (KBr, KCl and Na_2SO_4) on the γCD-AD complex. Other commonly used host molecule cucurbit[6]uril (CB6) was examined its ability of assisting α-HL with the stochastic sensing.[50] CB6 induced the reversible current blockages in the *cis* side of αHL. After the addition of tetrahydrofuran (THF), a clear increase of blockage current arises because of the complex αHL·CB6·THF. In βCD functionalized α-HL, the rate of exchange of guest molecule with its binding site within βCD is faster than the dissociation constant between βCD·guest and its binding site in the lumen of the pore.[42] However, the transitions between two current levels which contributed to the association and dissociation of THF from α-HL·CB6 were not detected. These results suggest that CB6 acts as a carrier in nanopore sensing rather than an adapter comparing to βCD·guest complex.

All the βCD, γCD and CB6 are suitable for lodging in the lumen of an α-HL. These host molecules acting as either the adapter or the carrier extend the range of analytes for an α-HL nanopore to small organic molecules. Since βCD, γCD and CB6 have the comparable diameters to the lumen of α-HL, it seems that the size of host molecule is the prerequisite for constructing a host-functionalized α-HL pore. However, the recent studies in our group showed that sulfonato-calix[4]arene (SC4), which is 7 times smaller than the narrowest part of the stem region associated with α-HL, could be used to functionalize the α-HL.[51] Our results demonstrated that SC4 induced a substantially higher inhibition of the ion current and even produced a full blockage of the pore. The inhibition of ion current flow through α-HL revealed a voltage as well as an orientational dependence. In the presence of SC4 at *trans* side of the pore, it induces a long-term close-state of α-HL at the holding potential more negative than -70 mV. The inter-event time-intervals of α-HL (τ_{on}) are inversely proportional to the applied holding potential from -70 mV to -140 mV as shown in Fig 4a, indicating that the probability to sustain the full open-state of α-HL is substantially lower with more negative holding potential. Furthermore, SC4 is repelled from the binding site by treating a repulsive potential across the membrane. The evidences above illustrated that the close-states of α-HL are mainly induced by strong host-guest interactions between the positive residues (probably Lys^{131} and Lys^{147}) of α-HL and negatively charged SC4.

By virtue of SC4 induced inhibition mechanisms, the SC4:α-HL can be commanded both by ligand and light stimuli. The light-sensitive 4, 4'-dipyridinium-azobenzene (V^{2+}-Az) was designed as a functional guest molecule (Fig. 4b). The binding constant between SC4 and *trans* state of V^{2+}-Az, (V^{2+}-*trans*-Az) is about 10^5 M^{-1}, two orders of magnitude larger than that of SC4: Lysine (K_a = 753 M^{-1}) at pH = 8. In the presence of V^{2+}-*trans*-Az, the inhibitions of SC4:α-HL system were rarely detected at the holding potential from -70 mV to -130 mV. When the holding potential negatively increased to -140 mV, the value of τ_{on} is 2.41 ± 0.14 ms, which is significantly larger than that for SC4 only at -140 mV (0.09 ± 0.04 ms). Therefore, the SC4 functionlized α-HL could be used to detect the competition between two guest molecules which are V^{2+}-*trans*-Az and the positive residues of α-HL (probably Lys^{131} or Lys^{147}). Since the light stimulates the association and dissociation of the respective photoisomers of V^{2+}-Az (V^{2+}-*trans*-Az/ V^{2+}-*cis*-Az) to and from the SC4, the frequency of inhibitions in the assay of V^{2+}-*cis*-Az was larger than that of V^{2+}-*trans*-Az (Fig. 4c). The SC4:α-HL system showed the photoismerization efficiency of V^{2+}- Az is 28%, comparable to the calculation from ^{1}H NMR which is about 33%. Further

experiments illustrated that this novel α-HL:SC4 system could real-time monitor the dynamic process for the photoisomerization of SC4: V^{2+}-Az at the single-molecule level (Fig. 4d). This study displayed a new strategy for construction of a host-functionalized nanopore system in which the host molecule could act as an inhibitor.
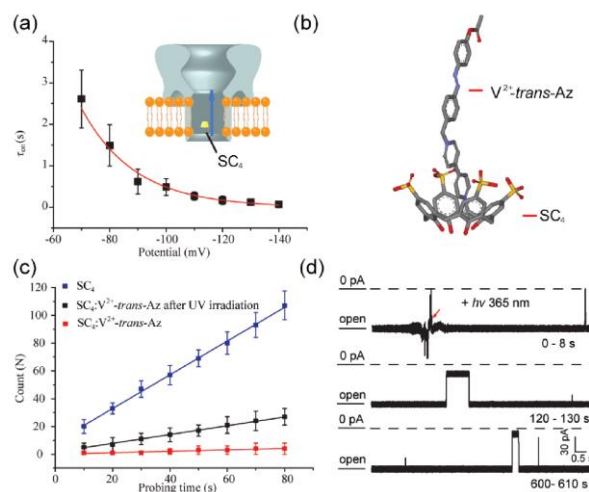

Fig. 4 (a) The effect of voltage on the the inter-event time-intervals of α-HL (τ_{on}) induced by SC4 from *trans* side. A large value of τ_{on} suggests that the inhibitions occur at a low frequency and vice versa. Insert: The model shows that SC4 is driven into the *trans* side of α-HL. (b) The representation of SC4:V^{2+}-*trans*-Az complex. (c) The number of blockages versus the probing time for SC4 (blue), SC4:V^{2+}-*trans*-Az after UV irradiation (black) and SC4:V^{2+}-*trans*-Az (red) at the potential of -100 mV. (d) Real-time monitoring the current traces induced by the photoisomerization of SC4:V^{2+}-Az by α-HL. Reproduced with the permission from Ref.51.

4. Analysis of the bumping events in nanopore detections

The analyte traverses through the nanopore and produces the distinguishable translocation blockages. If an analyte is larger than the constriction of biological nanopore, it would interact with the pore, and bounce back instead of translocation. This manner would generate the bumping events in most cases. By analyzing the duration and current distributions of the bumping events, the α-HL achieved to detect single molecule behavior of the analytes in large size, such as illuminating the interactions between prion proteins and metal ions[52, 53] and analyzing the aggregation states of peptides.[54-56]

A previous study showed that the aggregation states of β-amyloid 42 (Aβ42) could be analyzed by monitoring the bumping events using an α-HL nanopore (Fig. 5a-c).[54] Aβ42 is found in the plaques of the brains of Alzheimer's patients and its aggregated form is toxic to neuronal cells.[57] The addition of Aβ42 into the *cis* side of α-HL produces two types of events. As illustrated in Fig. 5b, the events with low-amplitude current have shorter durations while the events with a high-amplitude current have longer duration. The former events were interpreted as collisions of monomeric Aβ42 or self-aggregated fibrils against the *cis* entrance of the α-HL pore. The dissociated monomeric Aβ42 upon the addition of CR generates the long-lived events around 18 pA. (Fig. 5c). These events could be attributed to the horizontally captured monomeric Aβ42 and organized itself in the vestibule before transit
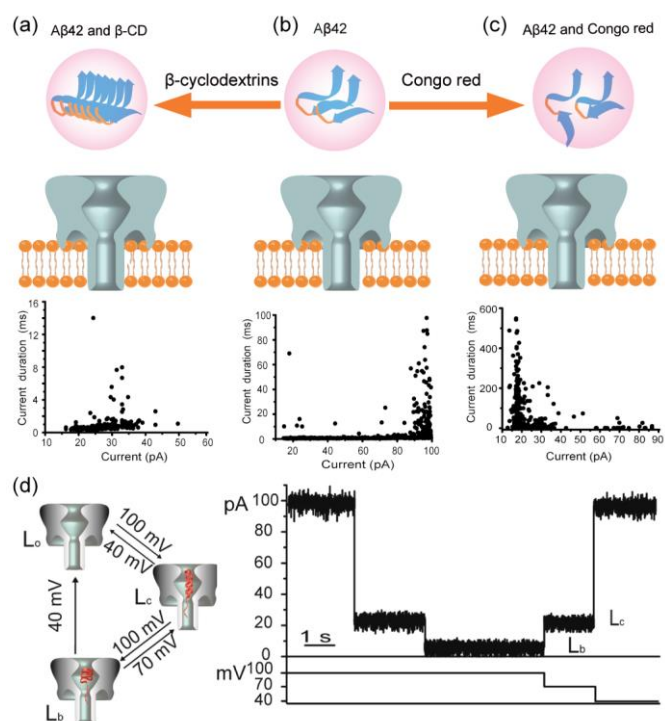
Fig. 5 Representations of the collision behavior and scatter plot of Aβ42-CD (a), Aβ42 (b) and Aβ42-CR (c), respectively. (d) The characteristic current blockage control by voltage change of a single α-syn molecule captured inside the vestibule. The three levels of blockage current defined as open pore current level (L$_o$), capture blockade current level (L$_c$), and block current level (L$_b$). Reproduced with the permission from Ref. 54 and 55

proportion of bumping events increased while the number of translocation events decreases. The aggregated Aβ42 is too large to translocate through the α-HL pore, which induces the short-lived events located around 50 pA (Fig. 5a). Therefore, the differences for the bumping events are related to the aggregation states caused by the interactions of CR and βCD with Aβ42.

The bumping events could be generated via regulating the applied potential across the membrane. By using this method, fibrils procedure of α-synuclein (α-syn) has been investigated by α-HL nanopore in the solution of 1 M NaCl (Fig. 5d).[55] The natively unfolded α-syn monomer transversed through α-HL pore by applying potential of +100 mV. When the potential is higher than +100 mV, a partially folded intermediate would be captured inside the vestibule of α-HL. At +70 mV, a further blocking of the intermediate produced a decrease in the blockage current, revealing that the early-stage fibril of α-syn is affected by intramolecular electrostatic interactions. After lowering the voltage to +40 mV, the captured intermediate exited from the vestibule. The manipulated bumping events as shown in Fig. 5d demonstrated that the intermediate of α-syn involves in its critical early stage of the structural transformation. Furthermore, the effect of trehalose used in the clearance of A53T α-syn protofilaments was conducted by monitoring the bumping events. This work provided unique insights into the early steps of α-syn aggregation pathway. The studies from Lee's group also showed that the differences in the bumping events could be used to detect the conformational changes of α-syn induced by the methamphetamine in the solution of KCl.[56]

5. Novel Biological Nanopores

As described above, the bumping events carried out by the wild

occurring. In contrast, increasing the incubation time of β-cyclodextrin (βCD) as an aggregation promoter with Aβ42, the
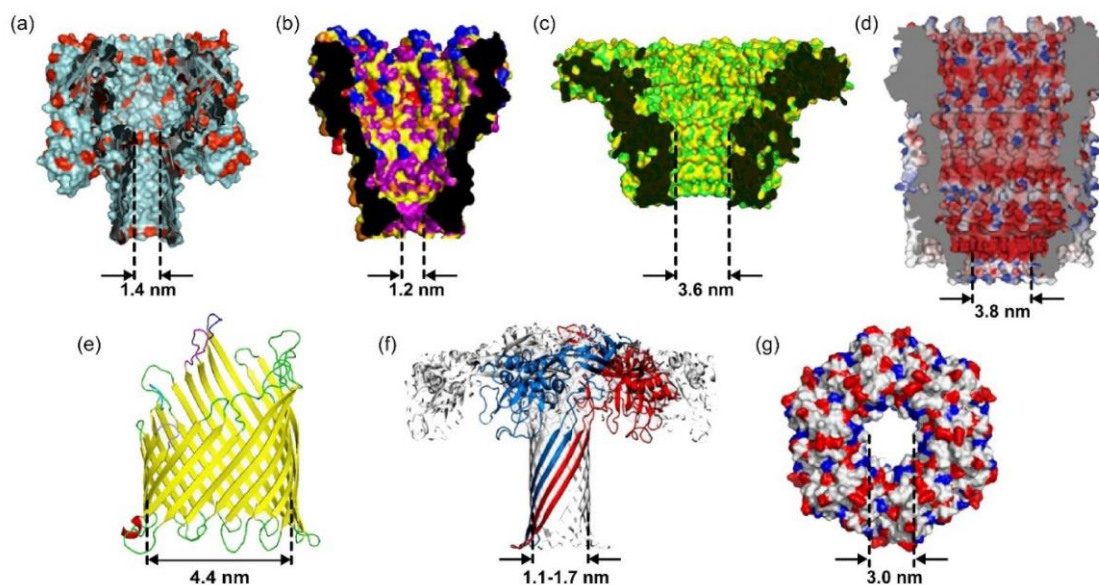

Fig. 6 The illustrations of biological nanopores used in the single-molecule detections. (a) α-HL (PDB: 7AHL)[51], (b) MspA[58]; (c) phi 29 DNA-packaging nanomotor (PDB: 1JNB); (d) ClyA[59]; (e) FhuA[60]; (f) aerolysin[61]; (g) SP1[62]. Reproduced with the permission from Ref. 51 and 58-62.

type of α-HL pore could be used to sense the aggregation states of peptides. However, it is difficult for the wild type α-HL to precisely examine the biomolecules which are larger than the

dimension of α-HL. On the other hand, the β-barrel of α-HL pore has a length around 5.2 nm, which could be occupied by around 20 nucleotides (Fig. 6a). When conducting the

nanopore-based DNA sequencing, it is difficult to differentiate the precise contribution of each base to the recorded blockage current. To overcome the limitations of α-HL pore, one strategy is to manipulate the dimensions of biological nanopores. Hence, various biological membrane proteins have been selected and engineered for biological nanopore sensors. *Mycobacterium smegmatis* porin A (MspA) attracts intensive attention in the field of nanopore-based DNA sequencing since it has a short and narrow constriction, ~ 1.2 nm wide and ~0.6 nm long (Fig. 6b).[63] Thus, the blockage current of MspA is affected by only four neighbouring nucleotides. The mutant MspA analysis of different homopolymer strands showed the conductance difference of as much as 0.23 nS[64], nearly ten times more separation than the results from α-HL pore (~ 0.028 nS)[65, 66]. A DNA strand is automated forward and reverse ratcheted by bacteriophage phi29 DNA polymerase in single-file order through MspA pore, which yields a well-resolved current signal with median durations of ~28 ms and current differences of up to 40 pA.[67] This method maped six different DNA sequences

with readable regions from 42 to 53 bases by reading the current signals.

The bacterial virus phi 29 DNA-packaging nanomotor acting as path for the translocation of double-strand DNA (dsDNA), has inspired its application in nanopore detections. As illustrated in Fig. 6c, the length of the connector is ~ 7nm, while the diameter of the channel is 3.6 nm at the narrow end and 6 nm at its wide end. The larger channel of phi 29 DNA-packaging nanomotor facilitates the single molecule analysis of dsDNA.[68, 69] The modification of the channel resulted in a sharper detection region for real-time detection of ssDNA. [70] The reengineering of the recognizing molecules within the large channel of phi 29 DNA-packaging nanomotor made it achieve the discrimination of chemicals and antibodies.[71, 72] Furthermore, other new types of biological channels including ClyA and FhuA (Fig. 6d-e) have also been selected and engineered for the purpose of sensing a large analyte, such as proteins.[73, 74] The types of biological nanopores have been summarized and listed in Table 1.

Table 1. Detection of analytes with biological nanopores

Biological Nanopore	Diameter [a] (nm)	Analyte	Comments	Reference [b]
α-HL	~ 1.4	Metal ions, small organics, RNA, ssDNA, amino acids, polymers, peptides, proteins, nanoparticles, etc.	Large-scale applications due to its reproducible structure and easy manipulation by site-directed mutagenesis.	1, 7, 9, 22, 31, 76-82
MspA	~ 1.2	ssDNA, dsDNA	Suitable geometry for nanopore DNA sequencing.	59, 62, 83, 84
Phi 29 DNA-packaging nanomotor	3.6	ssDNA, dsDNA, thioesters antibody	Allowing for the detection of larger analytes and offering more space for further modifications.	63, 64, 66, 67
ClyA	3.3	ssDNA, proteins	Suitable for the accommodation of small to medium-sized proteins within the nanopore lumen.	68, 85, 86
FhuA	~ 2.4	enzyme, protein-DNA interaction	Examining the proteolytic activity of an enzyme at pH 3.9 and determining the kinetics of protein−DNA aptamer interactions at physiological salt concentration.	69
aerolysin	1 ~ 1.7	peptides, proteins	Sensing of α-helix peptides and unfolded proteins.	71, 72, 73
SP1	~3	ssDNA	Analyzing of ssDNA	75

[a] The diameters for biological nanopores refer to their constrictions. A 12 mer oligomeric forms of ClyA has a diameter of 3.3 nm for its constriction. [b] The references for α-HL are selected, but not limited to.

As shown in Fig. 6f, the aerolysin nanopore which has an estimated diameter of 1 ~ 1.7 nm[75] has been welcomed in the single molecule studies of peptides[25, 76] and unfolded proteins[77, 78]. Aerolysin nanopores have been shown that the dipole moment and the net charge of each peptide has a major effect on the transport characteristics.[76] The ratio of translocation/bumping events increases as the dipole moment increases. Previous study demonstrated that duration time of MalEwt unfolded protein obtained in aerolysin were longer than those recorded with α-HL,[77] which ensured the higher time resolution of aerolysin nanopore in the studies of unfolded

peptide. Moreover, the unfolded states from partially folded proteins can also be distinguished by the aerolysin nanopore.[78]

To conduct the measurements in hash environment, the biological protein pores should withstand denaturants, extremes of the pH and temperatures. Stable protein 1 (SP1), a new boiling stable protein, has a high thermostability *i.e.* T_m of 107℃.[6] A spontaneous assembly of SP1 to form ring-like dodecamer could permeate into the bilayer.[62, 89] The structure of SP1 nanopore has an inner diameter of 3 nm and a pore length of 4-5 nm (Fig. 6g), which is suitable for the single biomolecule detection. Five sequences of ssDNA including poly(dA)$_{20}$, poly(dA)$_{45}$, poly(dT)$_{20}$, poly(dT)$_{45}$ and a multi-polynucleotide sequence were electrophoretically driven through the SP1 nanopore, respectively.[62] All of the five sequences showed

measurable current blockages by SP1 nanopore. For a homo-deoxyribonucleic polymer, the mean duration time of the ssDNA traversing through the pore relates to the length of ssDNA. For ssDNA with equal number of bases, the rigid chain of multi-polynucleotide sequence and poly(dA) translocated 2.5 times faster than poor stacking poly(dT). Therefore, SP1 could be used as a nanopore biosenosr to analyze the ssDNA. Since SP1 behaves the good thermostability and resistance to proteases of pore, it qualifies as an ideal material for the single molecule analysis in hash environment.

6. Conclusions

In conclusion, we have briefly reviewed the recent strategies for utilizing biological nanopore sensors. It should be noted that the incorporation of recognition probe such as aptamer and taking an advantage of host-guest interactions have greatly improved the selectivity and sensitivity of biological nanopores. To further achieve the precise analysis of an individual molecule, the recognition of analyte should be mutually confirmed by two types of read-outs which are electrical and optical signals if nanopore sensing is integrated with optical spectroscopy such as florescence, Raman scattering and plasmonic resonance.[90] The selection and engineering of various new types of biological pores benefits the biological nanopores with an extended application as well as withstanding for a measurement in hash environment. Furthermore, several obstacles need to be overcome in order to improve biological nanopore into a routine analytical tool in the single molecule analysis. First, the fragility of the biological membrane acts as a barrier for commercializing the biological nanopore probes. Previous studies reported that the lipid membrane layered within the agarose gel consistently retains a high-sealing property for a week.[91, 92] Further efforts may be made to overcome the fragility of the membrane by both creating the new type of lipid systems and reducing the size of aperture over which the lipid membrane is formed. Second, thousands of nanopore events are acquired within one minute in most of cases. At present, nanopore technique consumes plenty of time to discriminate and analyze the characteristic signals generated by the analyte from the large amounts of events. Therefore, it is necessary to develop data analyzing program to automatically and accurately process the signals, which will promote nanopore techniques to be mastered and utilized. Third, the whole device of biological nanopore including amplifier and A/D convertor should be portable and affordable for the on-site detections. However, most of the nanopore experiments are conducted on the patch clamp system which has a large size. A recent study fabricated a CMSO voltage-clamp current preamplifier which has a dimension of 3 mm * 3 mm.[93] The elegant design of the circuitry will facilitate nanopore sensing platform to become a personalized device or an *in vitro* diagnostic instrument. Moreover, the developments of instruments will accelerate nanopore technique toward an affordable and competitive single-molecule approach. With the continuing efforts from both experimental strategies and innovations of platforms, biological nanopore sensors will charm their applications in routine use of single molecule analysis.

Acknowledgements

Notes and references

Key Laboratory for Advanced Materials & Department of Chemistry, East China University of Science and Technology, P. R. China. E-mail: ytlong@ecust.edu.cn

1. J. Kasianowicz, E. Brandin, D. Branton and D. Deamer, *Proc. Natl. Acad. Sci. U. S. A.*, 1996, 93, 13770-13773.
2. L. Song, M. Hobaugh, C. Shustak, S. Cheley, H. Bayley and J. Gouaux, *Science*, 1996, 274, 1859-1865.
3. H. Bayley and C. R. Martin, *Chem. Rev.*, 2000, 100, 2575-2594.
4. D. W. Deamer and D. Branton, *Acc. Chem. Res.*, 2002, 35, 817-825.
5. H. Bayley and P. S. Cremer, *Nature*, 2001, 413, 226-230.
6. H. Bayley, O. Braha and L. Q. Gu, *Adv. Mater.*, 2000, 12, 139-142.
7. O. Braha, L. Q. Gu, L. Zhou, X. Lu, S. Cheley and H. Bayley, *Nat. Biotechnol.*, 2000, 18, 1005-1007.
8. T. Luchian, S. H. Shin and H. Bayley, *Angew. Chem. Int. Ed.*, 2003, 42, 3766-3771.
9. S. Howorka, J. Nam, H. Bayley and D. Kahne, *Angew. Chem. Int. Ed.*, 2004, 43, 842-846.
10. S. Loudwig and H. Bayley, *J. Am. Chem. Soc.*, 2006, 128, 12404-12405.
11. G. Maglia, A. J. Heron, D. Stoddart, D. Japrung and H. Bayley, Chapter 22 - Analysis of Single Nucleic Acid Molecules with Protein Nanopores, *Methods in Enzymology*, Academic Press, 2010, 475, 591-623.
12. D. Branton, D. W. Deamer, A. Marziali, H. Bayley, S. A. Benner, T. Butler, M. Di Ventra, S. Garaj, A. Hibbs and X. Huang, *Nat. Biotechnol.*, 2008, 26, 1146-1153.
13. A. E. Schibel, N. An, Q. Jin, A. M. Fleming, C. J. Burrows and H. S. White, *J. Am. Chem. Soc.*, 2010, 132, 17992-17995.
14. A. E. P. Schibel, A. M. Fleming, Q. Jin, N. An, J. Liu, C. P. Blakemore, H. S. White and C. J. Burrows, *J. Am. Chem. Soc.*, 2011, 133, 14778-14784.
15. N. An, A. M. Fleming, H. S. White and C. J. Burrows, *Proc. Natl. Acad. Sci. U. S. A.*, 2012, 109, 11504-11509.
16. Q. Jin, A. M. Fleming, C. J. Burrows and H. S. White, *J. Am. Chem. Soc.*, 2012, 134, 11006-11011.
17. Y. Wang, D. Zheng, Q. Tan, M. X. Wang and L. Q. Gu, *Nat. Nanotechnol.*, 2011, 6, 668-674.
18. K. Tian, Z. He, Y. Wang, S. J. Chen and L. Q. Gu, ACS Nano, 2013, 7, 3962-3969.
19. C. Yang, L. Liu, T. Zeng, D. Yang, Z. Yao, Y. Zhao and H.-C. Wu, *Anal. Chem.*, 2013, 85, 7302-7307.
20. S. Wen, T. Zeng, L. Liu, K. Zhao, Y. Zhao, X. Liu and H. C. Wu, *J. Am. Chem. Soc.*, 2011, 133, 18312-18317.
21. A. Oukhaled, L. Bacri, M. Pastoriza-Gallego, J. M. Betton and J. Pelta, *ACS Chem. Biol.*, 2012, 7, 1935-1949.
22. L. Movileanu, J. P. Schmittschmitt, J. Martin Scholtz and H. Bayley, *Biophys. J.*, 2005, 89, 1030-1045.
23. M. M. Mohammad and L. Movileanu, *Eur Biophys J*, 2008, 37, 913-925.
24. L. Movileanu, *Trends Biotechnol.*, 2009, 27, 333-341.

25. H. Y. Wang, Y. L. Ying, Y. Li and Y.-T. Long, *Chem.–Asian J.*, 2010, 5, 1952-1961.

26. J. E. Reiner, A. Balijepalli, J. W. Robertson, J. Campbell, J. Suehle and J. J. Kasianowicz, *Chem. Rev.*, 2012, 112, 6431-6451.

27. B. M. Venkatesan and R. Bashir, *Nat. Nanotechnol.*, 2011, 6, 615-624.

28. R. D. Maitra, J. Kim and W. B. Dunbar, *Electrophoresis*, 2012, 33, 1-11.

29. M. Wanunu, *Phys. Life Rev.*, 2012, 9, 125-158.

30. Y.-L. Ying, J. Zhang, R. Gao and Y.-T. Long, *Angew. Chem. Int. Ed.*, 2013, 52, 13154-13161.

31. J. J. Kasianowicz, S. E. Henrickson, H. H. Weetall and B. Robertson, *Anal. Chem.*, 2001, 73, 2268-2272.

32. S. E. Henrickson, M. Misakian, B. Robertson and J. J. Kasianowicz, *Phys. Rev. Lett.*, 2000, 85, 3057-3060.

33. S. E. Henrickson, E. A. DiMarzio, Q. Wang, V. M. Stanford and J. J. Kasianowicz, *J. Chem. Phys.*, 2010, 132, 135101.

34. Y. L. Ying, D. W. Li, Y. Li, J. S. Lee and Y.-T. Long, *Chem. Commun.*, 2011, 47, 5690-5692.

35. J. W. Shim and L. Q. Gu, *J. Phys.l Chem. B*, 2008, 112, 8354-8360.

36. L. Gu and J. Shim, *Analyst*, 2010, 135, 441-451.

37. Y. L. Ying, H. Y. Wang, T. C. Sutherland and Y. T. Long, *Small*, 2011, 7, 87-94.

38. D. Rotem, L. Jayasinghe, M. Salichou and H. Bayley, *J. Am. Chem. Soc.*, 2012, 134, 2781-2787.

39. X. Zhang, J. Zhang, Y. Yi-Lun, H. Tian and Y.-T. Long, *Chem. Sci.*, 2014, DOI: 10.1039/C1034SC00134F.

40. D. D. Young and A. Deiters, *ChemBioChem*, 2008, 9, 1225-1228.

41. R. Kawano, T. Osaki, H. Sasaki, M. Takinoue, S. Yoshizawa and S. Takeuchi, *J. Am. Chem. Soc.*, 2011, 133, 8474-8477.

42. L. Q. Gu, O. Braha, S. Conlan, S. Cheley and H. Bayley, *Nature*, 1999, 398, 686-690.

43. L.-Q. Gu and H. Bayley, *Biophys. J.*, 2000, 79, 1967-1975.

44. L. Q. Gu, S. Cheley and H. Bayley, *Science*, 2001, 291, 636-640.

45. Y. Astier, O. Braha and H. Bayley, *J. Am. Chem. Soc.*, 2006, 128, 1705-1710.

46. H.-C. Wu, Y. Astier, G. Maglia, E. Mikhailova and H. Bayley, *J. Am. Chem. Soc.*, 2007, 129, 16142-16148.

47. J. Clarke, H. C. Wu, L. Jayasinghe, A. Patel, S. Reid and H. Bayley, *Nat. Nanotechnol.*, 2009, 4, 265-270.

48. W. W. Li, T. D. Claridge, Q. Li, M. R. Wormald, B. G. Davis and H. Bayley, *J. Am. Chem. Soc.*, 2011, 133, 1987-2001.

49. P. A. Gurnev, D. Harries, V. A. Parsegian and S. M. Bezrukov, *ChemPhysChem*, 2009, 10, 1445-1449.

50. O. Braha, J. Webb, L. Q. Gu, K. Kim and H. Bayley, *ChemPhysChem*, 2005, 6, 889-892.

51. Y.-L. Ying, J. Zhang, F.-N. Meng, C. Cao, X. Yao, I. Willner, H. Tian and Y.-T. Long, *Sci. Rep.*, 2013, 3, 1662.

52. B. Krasniqi and J. S. Lee, *Metallomics*, 2012, 4, 539-544.

53. R. I. Stefureac, C. A. Madampage, O. Andrievskaia and J. S. Lee, *Biochem. Cell Biol.*, 2010, 88, 347-358.

54. H. Y. Wang, Y. L. Ying, Y. Li, H. B. Kraatz and Y.-T. Long, *Anal. Chem.*, 2011, 83, 1746-1752.

55. H. Y. Wang, Z. Gu, C. Cao, J. Wang and Y. T. Long, *Anal. Chem.*, 2013, 85, 8254-8261.

56. O. Tavassoly and J. S. Lee, *FEBS Lett.*, 2012, 586, 3222-3228.

57. P. Inbar, M. R. Bautista, S. A. Takayama and J. Yang, *Anal. Chem.*, 2008, 80, 3502-3506.

58. I. M. Derrington, T. Z. Butler, M. D. Collins, E. Manrao, M. Pavlenok, M. Niederweis and J. H. Gundlach, *Proc. Natl. Acad. Sci. U. S. A.*, 2010, 107, 16060-16065.

59. M. Mueller, U. Grauschopf, T. Maier, R. Glockshuber and N. Ban, *Nature*, 2009, 459, 726-730.

60. M. M. Mohammad, R. Iyer, K. R. Howard, M. P. McPike, P. N. Borer and L. Movileanu, *J. Am. Chem. Soc.*, 2012, 134, 9521-9531.

61. M. T. Degiacomi, I. Iacovache, L. Pernot, M. Chami, M. Kudryashev, H. Stahlberg, F. G. van der Goot and M. Dal Peraro, *Nat. Chem. Biol.*, 2013, 9, 623-629.

62. H. Y. Wang, Y. Li, L. X. Qin, A. Heyman, O. Shoseyov, I. Willner, Y. T. Long and H. Tian, *Chem. Commun.*, 2013, 49, 1741-1743.

63. M. Faller, M. Niederweis and G. E. Schulz, *Science*, 2004, 303, 1189-1192.

64. E. A. Manrao, I. M. Derrington, M. Pavlenok, M. Niederweis and J. H. Gundlach, *PLoS One*, 2011, 6, e25723.

65. D. Stoddart, A. J. Heron, E. Mikhailova, G. Maglia and H. Bayley, *Proc. Natl. Acad. Sci. U. S. A.*, 2009, 106, 7702-7707.

66. R. F. Purnell, K. K. Mehta and J. J. Schmidt, *Nano Lett.*, 2008, 8, 3029-3034.

67. E. A. Manrao, I. M. Derrington, A. H. Laszlo, K. W. Langford, M. K. Hopper, N. Gillgren, M. Pavlenok, M. Niederweis and J. H. Gundlach, *Nat. Biotechnol.*, 2012, 30, 349-353.

68. D. Wendell, P. Jing, J. Geng, V. Subramaniam, T. J. Lee, C. Montemagno and P. Guo, *Nat. Nanotechnol.*, 2009, 4, 765-772.

69. M. B. Wabuyele, S. M. Ford, W. Stryjewski, J. Barrow and S. A. Soper, *Electrophoresis*, 2001, 22, 3939-3948.

70. J. Geng, S. Wang, H. Fang and P. Guo, *ACS Nano*, 2013, 7, 3315-3323.

71. S. Wang, F. Haque, P. G. Rychahou, B. M. Evers and P. Guo, *ACS Nano*, 2013, 7, 9814-9822.

72. F. Haque, J. Lunn, H. Fang, D. Smithrud and P. Guo, *ACS Nano*, 2012, 6, 3251-3261.

73. M. Soskine, A. Biesemans, B. Moeyaert, S. Cheley, H. Bayley and G. Maglia, *Nano Lett.*, 2012, 12, 4895-4900.

74. M. M. Mohammad, R. Iyer, K. R. Howard, M. P. McPike, P. N. Borer and L. Movileanu, *J. Am. Chem. Soc.*, 2012, 134, 9521-9531.

75. M. W. Parker, J. T. Buckley, J. P. Postma, A. D. Tucker, K. Leonard, F. Pattus and D. Tsernoglou, *Nature*, 1994, 367, 292-295.

76. R. Stefureac, Y. Long, H. B. Kraatz, P. Howard and J. S. Lee, *Biochemistry*, 2006, 45, 9172-9179.

77. M. Pastoriza-Gallego, L. Rabah, G. Gibrat, B. Thiebot, F. G. van der Goot, L. Auvray, J. M. Betton and J. Pelta, *J. Am. Chem. Soc.*, 2011, 133, 2923-2931.

78. C. Merstorf, B. Cressiot, M. Pastoriza-Gallego, A. Oukhaled, J. M. Betton, L. Auvray and J. Pelta, *ACS Chem. Biol.*, 2012, 7, 652-658.

79. S. Lu, W.-W. Li, D. Rotem, E. Mikhailova and H. Bayley, *Nature Chem.*, 2010, 2, 921-928.

80. Y. Liu, Y.-L. Ying, H.-Y. Wang, C. Cao, D.-W. Li, W.-Q. Zhang and Y.-T. Long, *Chem. Commun.*, 2013, 49, 6584-6586.

81. T. Luchian, S. H. Shin and H. Bayley, *Angew. Chem. Int. Ed.*, 2003, 42, 3766-3771.

82. J. W. Robertson, C. G. Rodrigues, V. M. Stanford, K. A. Rubinson, O. V. Krasilnikov and J. J. Kasianowicz, *Proc. Natl. Acad. Sci. U. S. A.*, 2007, 104, 8207-8211.

83. X.-F. Kang, S. Cheley, X. Guan and H. Bayley, *J. Am. Chem. Soc.*, 2006, 128, 10684-10685.

84. T. C. Sutherland, M. J. Dinsmore, H. B. Kraatz and J. S. Lee, *Biochem. Cell Biol.*, 2004, 82, 407-412.

85. Y. Astier, O. Uzun and F. Stellacci, *Small*, 2009, 5, 1273-1278.

86. T. Z. Butler, M. Pavlenok, I. M. Derrington, M. Niederweis and J. H. Gundlach, *Proc. Natl. Acad. Sci. U. S. A.*, 2008, 105, 20647-20652.

87. L. Franceschini, M. Soskine, A. Biesemans and G. Maglia, *Nat. Commun., 2013, 4, 2415.*

88. M. Soskine, A. Biesemans, M. De Maeyer and G. Maglia, *J. Am. Chem. Soc.*, 2013, 135, 13456-13463.

89. W.-X. Wang, D. Pelah, T. Alergand, O. Shoseyov and A. Altman, *Plant Physiol.*, 2002, 130, 865-875.

90. B. McNally, A. Singer, Z. Yu, Y. Sun, Z. Weng and A. Meller, *Nano Lett.*, 2010, 10, 2237-2244.

91. J. W. Shim and L. Q. Gu, *Anal. Chem.*, 2007, 79, 2207-2213.

92. X.-F. Kang, S. Cheley, A. C. Rice-Ficht and H. Bayley, *J. Am. Chem. Soc.*, 2007, 129, 4701-4705.

93. J. K. Rosenstein, M. Wanunu, C. A. Merchant, M. Drndic and K. L. Shepard, *Nat. Methods*, 2012, 9, 487-492.

Analyst Accepted Manuscript